(650

1. SPIN-POLARIZED ELECTRON SOURCES

Daniel T. Pierce

Electron Physics Group, National Institute of Standards and Technology,
Gaithersburg, Maryland

1.1 Introduction

Most polarized electron sources in use today are based on photoemission from negative-electron-affinity (NEA) semiconductor photocathodes, such as GaAs and related compounds, and thus these form the central focus of this chapter. It is worth noting at the outset that, in addition to producing spin-polarized beams, these photocathodes have other advantageous features, such as their high brightness, narrow energy spread of the emitted beam, and the possibility of modulating the beam intensity with an arbitrary time structure by controlling the photoexciting light. The experimental techniques presented in this chapter for electron guns with NEA photocathodes are also relevant for such guns in their numerous applications beyond those involving spin polarization.

Because there is no simple polarization filter for electrons equivalent to a calcite prism for light or a Stern–Gerlach magnet for atoms, a number of spin-dependent processes have been tried in attempts to produce beams of spin-polarized electrons [1,2]. Chief among these are photoionization of polarized Li atoms [3], the Fano effect in Rb [4] and Cs [5], field emission from W–EuS tips [6], photoemission from the ferromagnetic crystal EuO [7], scattering from an unpolarized target [1], chemi-ionization of optically oriented metastable He [8–11], and photoemission from NEA GaAs. For most applications, photoemission from NEA GaAs and related materials provides the most suitable source of polarized electrons. The source based on chemi-ionization of metastable He is competitive for applications which require high polarization in a continuous beam of moderate intensity and has the further advantage that ultrahigh vacuum is not required. Some characteristics of this source will be discussed in Section 1.6.

Photoemission of optically oriented electrons from NEA GaAs as a source of polarized electrons was proposed in the mid-1970s [12,13]. The feasibility of the GaAs-polarized electron source was demonstrated in spin-polarized photoemission experiments at the ETH—Zurich [14–17].

EXPERIMENTAL METHODS IN THE PHYSICAL SCIENCES
Vol. 29A

The first polarized electron guns were developed for low-energy condensed matter experiments at the National Institute of Standards and Technology (NIST) [18] and for high-energy physics experiments at the Stanford Linear Accelerator Center (SLAC) [19], where the GaAs source was a crucial part of the landmark parity violation experiment of Prescott *et al.* [20,21]. The condensed matter experiments required a low-energy, continuous source while the high-energy parity-violation experiment required a pulsed beam with high initial injection energy. Although there are some fundamental differences in source design, there are also a number of similarities. There have been a number of advances in the GaAs-type sources over the years which can be attributed in large part to the demanding requirements on polarized electron sources for accelerator applications. An account of this progress is summarized in the reports [22–25] on a series of workshops on polarized sources for accelerators.

This chapter attempts to distill the advances in GaAs-polarized electron source technology, to present important information and considerations for someone building such a source, and to compare its performance with that of other polarized electron sources. A source of spin-polarized electrons can be characterized by a number of parameters which allow one to determine how well it will meet the requirements of a particular application. Foremost among these is the polarization itself which we define as $P = (N\uparrow - N\downarrow)/(N\uparrow + N\downarrow)$, where $N\uparrow$ ($N\downarrow$) are the number of electrons with spins parallel (antiparallel) to a quantization direction. The ideal polarized electron source would produce a beam with the maximum polarization, $P = \pm 1$. In Section 1.2, the physics behind production of polarized electrons in photoemission from GaAs is reviewed and the progress toward obtaining a fully polarized electron beam is discussed. For a source producing an electron beam of current I, the quantity P^2I is a useful figure of merit when counting statistics are the chief source of experimental uncertainty. It is sometimes possible to trade off polarization and increase the current I, but the current may also be limited, for example, by space-charge or target damage considerations. The current available with a given light source is determined by the quantum efficiency which depends on the cathode material, how the surface is cleaned, and how it is activated, as presented in Section 1.3. An important consideration in the construction of a polarized electron gun, as discussed in Section 1.4, is the control of the incident radiation to determine the time structure of the electron beam intensity and, because many experiments involve measuring a small spin-dependent asymmetry, to reverse the sign of the electron spin polarization without affecting other beam parameters such as intensity, angle, or position. Electron optical properties of the beam of photoelectrons extracted from the GaAs photocathode, such as the beam brightness and emittance discussed in Section 1.5, set limits on the parameters of the beam which can be obtained at the target in a particular application. In Section 1.6, the main features of the GaAs source are summarized and compared with those of other polarized electron sources.

1.2 Background

Photoemission from NEA GaAs can be described in a particularly straightforward way by Spicer's three-step model: photoexcitation, transport, and escape [26,27]. The polarized electrons are generated in the photoexcitation process. The transport and escape strongly affect the quantum efficiency (i.e., the number of electrons emitted per incident photon) as well as the depolarization of the electrons. There are a number of experimental challenges in constructing such a spin-polarized electron source, but two paramount ones are optimizing the polarization and optimizing the emitted current. A brief description of the theory of the GaAs-polarized electron source which will form the framework for discussing the experimental approaches to obtaining the desired performance is presented.

1.2.1 Optical Spin Orientation

GaAs is a direct gap semiconductor with a minimum band separation, E_g, at Γ as in the $E(k)$ plot of the energy bands vs crystal momentum k shown in the left side of Figure 1. The conduction band is a twofold degenerate $s_{1/2}$ level. The spin–orbit interaction splits the sixfold degenerate p state of the valence band maximum into a fourfold degenerate $p_{3/2}$ level and a twofold degenerate $p_{1/2}$ level lying 0.34 eV lower in energy. The fourfold degenerate $p_{3/2}$ level consists of the heavy-hole band with $m_j = \pm\frac{3}{2}$ and the higher curvature light-hole band with $m_j = \pm\frac{1}{2}$. The transitions for circularly polarized light σ^+ (σ^-) between the m_j sublevels are shown by solid (dashed) lines on the right side of the figure. The selection rules require that $\Delta m_j = +1$ or $\Delta m_j = -1$ for σ^+ or σ^- light, respectively. The Clebsch–Gordan coefficients give the relative intensities of these transitions. Thus for σ^+ light, the theoretical polarization is

$$P_{th} = (1 - 3)/(1 + 3) = -0.5. \tag{1.1}$$

With increasing photon energy, transitions from the split-off $p_{1/2}$ level eventually contribute with a relative intensity of 2, and the polarization is reduced to zero.

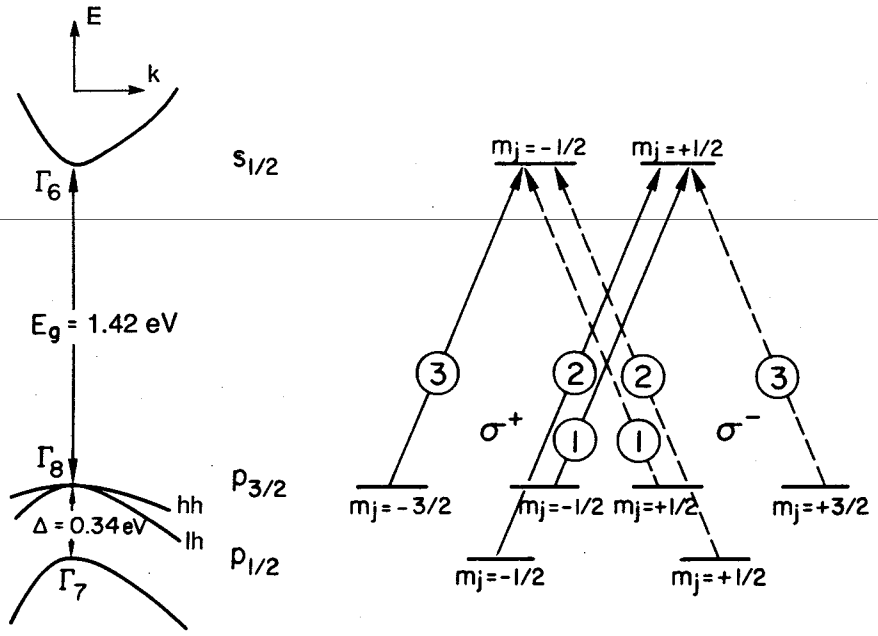

FIG. 1. The energy bands, $E(k)$, of GaAs near the center of the Brillouin zone are shown at the left of the figure. The room temperature bandgap is E_g = 1.42 eV, and the spin–orbit splitting of the valence bands is 0.34 eV. At the right, the allowed transitions between the m_j sublevels, for σ^+ and σ^- light are shown by the solid and dashed arrows, respectively. The circled numbers give the relative intensities. The degeneracy of the heavy-hole (hh) and light-hole (lh) bands at the valence band maximum limits the maximum polarization to −0.5 and +0.5 for σ^+ and σ^-, respectively. From Pierce and Meier [16].

1.2.2 Transport, Escape, and Depolarization

Ordinarily, the electrons excited to the conduction band minimum would be approximately 4 eV below the vacuum level and could not escape from the GaAs. By treating the surface of *p*-type GaAs with Cs and O_2, it is possible to lower the vacuum level at the surface below the energy of the conduction band minimum in the bulk to achieve the condition known as NEA [28]. This situation is illustrated in Figure 2. Instead of the escape depth being limited by the short mean-free path for inelastic scattering of hot electrons, the electrons from an NEA cathode are emitted from a depth determined by the diffusion length, L, which is on the order of 1 μm and comparable to the absorption length of the light, $1/\alpha$. The photoelectrons thermalize to the conduction band minimum in a time on

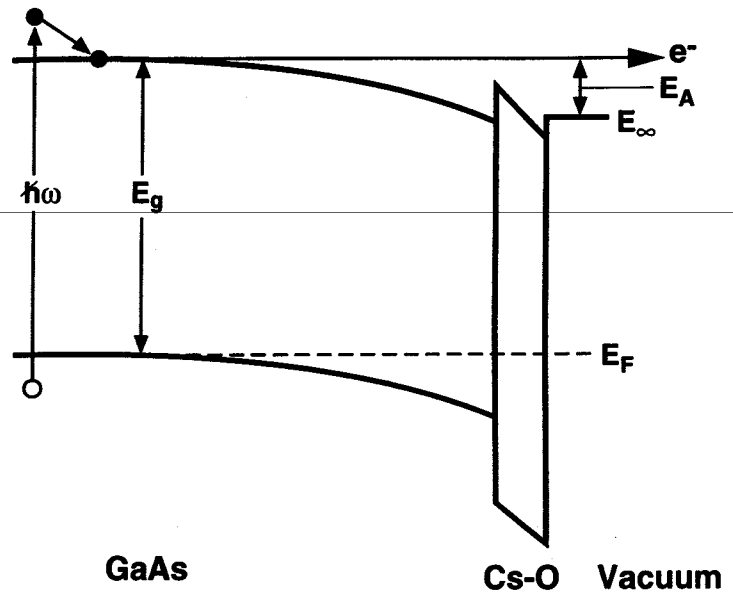

FIG. 2. The valence and conduction bands of *p*-type GaAs bend down at the surface. Activation with Cs and O_2 lowers the vacuum level E_∞ at the surface below the conduction band in the bulk, leading to an effective negative electron affinity, E_A. Electrons excited from the valence bands by photons of energy $\hbar\omega$ thermalize to the conduction band minimum and diffuse toward the surface, where they are accelerated in the band-bending region and escape into vacuum. From Pierce *et al.* [18].

the order of 10^{-12} sec and then diffuse toward the surface, where they are accelerated in the band-bending region, the width of which is determined by the doping level. When the electron reaches the surface, it can escape into vacuum or it may be reflected. A reflected electron may get turned around by scattering with phonons for subsequent attempts to escape at the surface. It may also recombine with a hole before it escapes. The probability that an electron which reaches the band-bending region is finally emitted is P_{esc}. For an NEA photocathode, the quantum efficiency or quantum yield, Y, is simply obtained in the three-step model in terms of these parameters as [26,27]

$$Y = P_{esc}/[1 + (\alpha L)^{-1}]. \tag{1.2}$$

This equation is valid for photon energies near E_g so that electrons thermalize into the Γ minimum rather than the higher-lying band minima [29]. For maximum yield, the light should be absorbed in a depth smaller than

the diffusion length. The diffusion length can be increased from about 0.5–1 μm in a bulk GaAs crystal to 3 μm or more in epitaxially grown material with few defects. One has less control over the absorption coefficient α which depends on the electronic structure of GaAs. The factor which affects the yield most strongly is the escape probability P_{esc} which depends sensitively on the surface preparation, that is, the cleaning and activation.

The minority carrier lifetime, τ, of a photoexcited electron diffusing in GaAs is directly related to L through the diffusion constant D with $L = (D\tau)^{1/2}$. As the electrons diffuse to the surface, they can become depolarized by a number of mechanisms [30] which can be characterized by a spin relaxation time, τ_s. The polarization of the photoemitted electrons P can be related to the larger theoretical polarization P_{th} by

$$P = P_{th}[\alpha + (D\tau)^{-1/2}]/[\alpha + (DT)^{-1/2}], \tag{1.3}$$

where $T = \tau_s\tau/(\tau_s + \tau)$ and approximations about the surface recombination velocity appropriate for an NEA cathode and a spin-independent escape probability have been assumed [18]. The equilibrium polarization of the photoexcited electrons inside the GaAs, P_L, as would be inferred from a photoluminescence measurement, is also less than P_{th} because electrons may undergo spin relaxation before they recombine. The polarization of photoemitted electrons has a direct relation to the equilibrium polarization, assuming no further depolarization in the escape through the activation layer,

$$P \approx [(\tau_s + \tau)/\tau_s]^{1/2} P_L. \tag{1.4}$$

Photoemitted electrons spend less time in the sample and hence have less time to depolarize than electrons which remain in the sample until they recombine; this leads to a photoelectron polarization which is higher than the equilibrium polarization as has been shown experimentally [31].

1.2.3 Optimizing the Polarization

Optimizing the polarization would be synonymous with "increasing" the polarization if that could be accomplished without adversely affecting other source characteristics. From the above discussion, it should be possible to increase the polarization toward P_{th} by artificially constructing a cathode with an active semiconductor layer that is very thin, since the less time photoexcited electrons remain in the GaAs, the less time they have to depolarize. Indeed, the polarization of photoemitted electrons from molecular beam epitaxy (MBE)-grown GaAs layers 0.2 μm thick was 0.49, near the theoretical maximum, but for 1-μm-thick layers the

polarization decreased to approximately 0.4 [32]. However, the higher polarization from the thinner active semiconductor layer was achieved at the sacrifice of quantum efficiency, since the light is absorbed over a distance much greater than the layer thickness. For thick GaAs cathodes, the measured polarizations range from roughly 0.25 to 0.4 depending on starting material, activation, and temperature. The causes of the differences in the reported polarizations are not entirely understood, although the difficulty in making accurate polarization measurements may also play a role.

The maximum polarization attainable from GaAs, $P_{th} = 0.5$, is a serious limitation. To obtain a higher P_{th} the degeneracy of the light-hole and heavy-hole bands at the valence band maximum must be lifted by reducing the symmetry of these states. This can be accomplished by: (1) choosing a material of lower crystal symmetry, such as a II–IV–V_2 chalcopyrite semiconductor like $CdSiAs_2$, (2) introducing strain in the emitting semiconductor layer, and (3) introducing periodic potential wells as in a GaAs–AlGaAs superlattice. The first measurements of spin-polarized photoelectrons from semiconductors with the chalcopyrite structure did not give high polarization [33]. Single crystal platelets of $CdSiAs_2$ [34] and $Zn(Ge_{0.7}Si_{0.3})As_2$ films grown by metal–organic chemical vapor deposition (MOCVD) [35] were successfully activated at or near NEA, but the measured polarizations did not exceed 0.2 even though $P_{th} = 1$. It is not known whether hybridization of the electron states or a shortcoming in the crystal preparation or activation is to blame for the large difference between theory and experiment for crystals with the chalcopyrite structure.

The first significant enhancement of the photoelectron spin polarization above 0.5 from an NEA photocathode was obtained using a strained $In_xGa_{1-x}As$ layer, with $x \approx 0.13$, grown on a GaAs substrate [36]. When the lattice constant of the substrate is less than the epilayer, as shown schematically in Figure 3a, there is a compressive biaxial strain in the plane of the layer and a tensile strain perpendicular to the layer. The lattice constant of GaAs is about 0.9% less than the $In_xGa_{1-x}As$ epilayer, resulting in a strain which causes the heavy-hole band to move up in energy and the light-hole band to move down as shown in Figure 3b. Theoretically, with σ^+ light of the proper photon energy, one has only the transition from $m_j = -\frac{3}{2}$ to $m_j = -\frac{1}{2}$, giving $P = -1$. The splitting δ of the light-hole and heavy-hole bands is proportional to the strain which is proportional to the In fraction x. For thin layers, the lattice mismatch is accommodated by elastic strain, but above a critical thickness, dislocations begin to relax the strain. Equilibrium thermodynamic arguments [37] predict a critical thickness on the order of 10 nm for InGaAs with $x = 0.13$. However, the strain is not significantly relaxed until a thickness

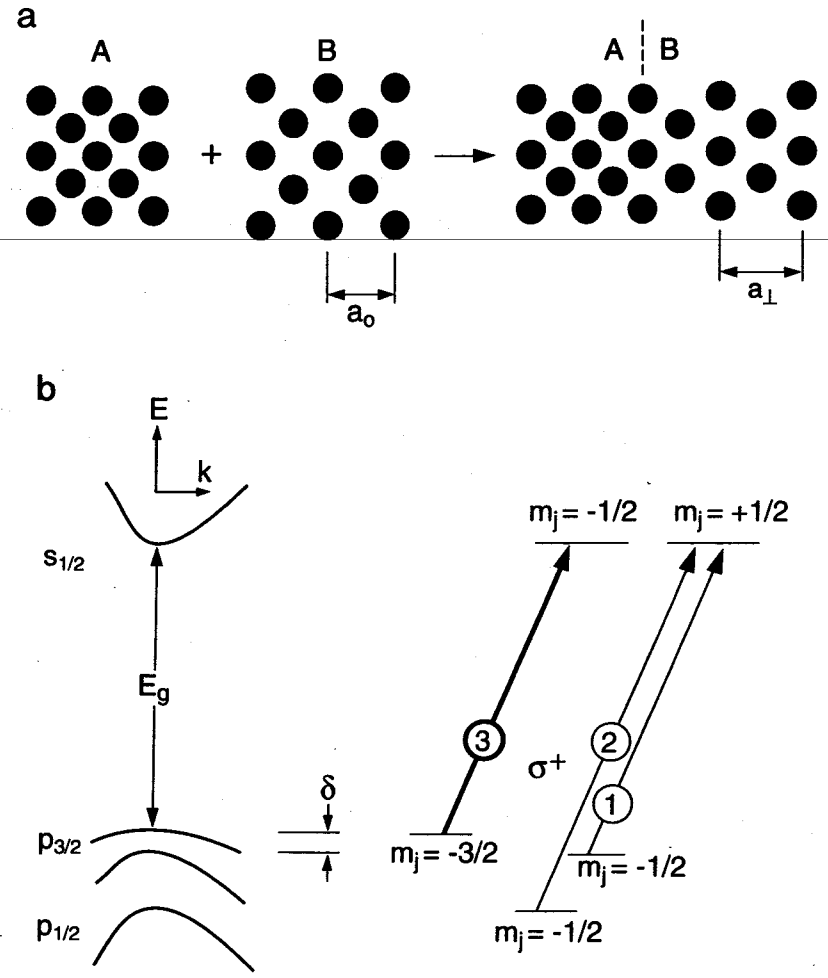

FIG. 3. (a) Schematic showing the growth of epilayer B on substrate A which has a smaller lattice constant. There is a compressive biaxial strain in the plane of the layer and a tensile strain perpendicular to the layer such that $a_\perp > a_0$. The pictured strain is about a factor of 25 greater than typical. (b) E vs. k band diagram showing how strain splits the heavy-hole and light-hole bands by an energy, δ, thus lifting the degeneracy. The allowed transitions for σ^+ light are shown on the right. Choosing the photon energy to select the transition shown by the heavy arrow gives $P = -1$.

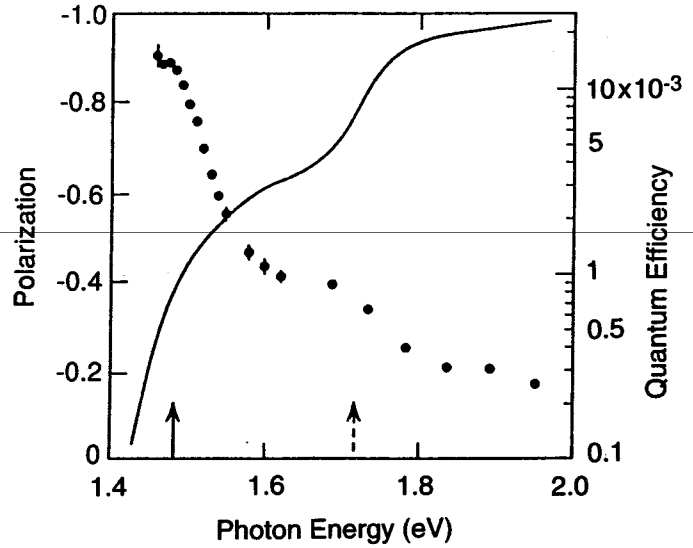

FIG. 4. Electron spin polarization (data points) and photocathode quantum efficiency (solid curve) as a function of excitation photon energy for GaAs grown on $GaAs_{1-x}P_x$ with $x = 0.28$. The calculated heavy-hole band gap is shown by the solid arrow, and the band gap of $GaAs_{1-x}P_x$ is shown by the dashed arrow. From Maruyama *et al.* [41].

approximately an order of magnitude larger is reached [38]. This result is very important, because a thicker layer leads to a higher quantum efficiency. Even though some of the light still passes through the active layer, the substrate has a larger band gap and does not contribute to the photocurrent until higher photon energies are reached.

Enhanced photoelectron spin polarization has also been observed in photoemission from strained GaAs layers grown on $GaAs_{1-x}P_x$ which has a smaller lattice constant than GaAs [39]. The dependence of spin polarization on strain has been investigated for this system [40,41]. Polarizations as high as 0.90 have been observed, and polarizations greater than 0.80 with a quantum efficiency greater than 0.1% have been achieved just above the heavy-hole band-gap energy indicated by the solid arrow in Figure 4 [41]. The dashed arrow shows the photon energy at which excitations in the GaAsP substrate begin to contribute and lead to an increase in quantum efficiency but a decrease in polarization.

A factor limiting the performance of strained-layer photocathodes is the limitation on the thickness required to prevent strain relaxation. Most

of the incident light goes right through the active layer, and the quantum efficiency is low. A novel approach [42a] to get around this deficiency has been suggested: the cathode is engineered to include a distributed Bragg reflector between the GaAs substrate and the GaAsP layer, thus forming a Fabry–Perot cavity with the surface of the strained GaAs epilayer. By tuning the wavelength of resonant absorption, an increase in quantum efficiency of an order of magnitude may be achieved without apparent loss of electron spin polarization [42a]. Some caution is suggested, however, by subsequent measurements of a similar cathode structure which revealed reductions in polarization to nearly zero over a narrow wavelength range in the region of maximum quantum efficiency; this was attributed to optical anisotropies caused by a small anisotropy of the in-plane lattice strain [42b].

Another way to remove the degeneracy of the heavy- and light-hole bands is to confine the electrons in quantum wells in a superlattice. Early attempts to increase the polarization above 50% by using a superlattice were not successful. A significant enhancement of the photoelectron polarization to 71% was later achieved [43]. The key parameters are the fraction of Al in the AlGaAs and the thickness of the GaAs and AlGaAs layers to obtain a large enough splitting of the heavy- and light-hole bands compared with thermal energies. The overall thickness of the superlattice must be small enough to minimize depolarization within the structure. The successful results were obtained from a superlattice with repeats of a 3.11-nm $Al_{0.35}Ga_{0.65}As$ layer and a 1.98-nm GaAs layer for an overall thickness of 0.1 μm. For this structure the heavy-hole band is calculated to be 44 meV higher in energy than the light-hole band. The reported [43] quantum efficiency at the highest polarization was 2.7×10^{-6}. Further studies [44] of superlattice cathodes showed that the polarization can be increased by reducing the p doping within the structure to 1×10^{17} cm^{-3} and increasing the thickness of the top GaAs layer to 5 nm with a p doping of 5×10^{18} cm^{-3}. This yielded a polarization of $P \geq 0.7$ and a quantum efficiency of 0.02.

These specialized custom-engineered strained-layer or superlattice photocathodes will not be the choice for the average builder of a polarized electron source. Such specialized cathodes either are very costly to purchase commercially or require close collaboration with a group which can grow such materials. They are described here to show the range of possibilities that exist and to illustrate the beautiful results which have been obtained as a result of efforts to increase the electron spin polarization. Such photocathodes are being used in demanding high-energy physics experiments.

1.3 The Photocathode

The photocathode material and its preparation are key to the polarized electron source. The material can be as simple as a bulk wafer or as complex as the sophisticated structures engineered to obtain high polarization. The quantum efficiency depends on the diffusion length, a material property, and is also very significantly determined by how the surface is cleaned and activated. The quantum efficiency for a bulk crystal or thick epilayer can range from typical values in the neighborhood of 3% obtained in most research laboratories to around 30% which is not unusual for cathodes prepared commercially by proprietary processes. We present two approaches to preparing photocathodes for polarized electron sources: (1) a known, reliable method which gives cathodes with the lower quantum efficiency, but which are still quite adequate for most applications (we label these "adequate" cathodes), and (2) some considerations for obtaining the higher quantum efficiency cathodes (we label these "optimum" cathodes). High-quantum-efficiency cathodes that optimize the electron escape probability may be important in cases in which the incident light intensity must be limited or in which the thickness of the photocathode layer is constrained.

1.3.1 Material

A direct gap III–V semiconductor, such as GaAs or a related material, has the energy level scheme, shown in Figure 1, required to generate spin-polarized photoelectrons. In addition to GaAs, InGaAs [36], GaAsP [45,46], and AlGaAs [47] have been used. The Al and P concentrations in the last two materials were chosen to obtain a band gap appropriate for photoexcitation with a HeNe laser at 1.96 eV. The larger band gap leads to a larger negative electron affinity. This larger NEA has been reported to help achieve long cathode lifetimes [48], but the photoelectron energy distributions were also observed to narrow as the NEA decreased with time [46].

The (100), (110), and (111) faces of p-type GaAs can all be activated to NEA [49], and all have been shown to emit polarized photoelectrons [50]. Best results are obtained for crystals doped from 5×10^{18} to 2×10^{19} cm^{-3}. Wafers with (100) surface orientation are commonly used as substrates for epitaxy and are readily available. The (110) GaAs cleavage planes are perpendicular to the (100) surface. The (100) wafers, which are typically a few tenths of a millimeter thick, are easily cleaved into rectangular pieces by pressing a fine knife on the upper edge of the wafer.

The (100) surface is recommended when using a bulk (that is, sliced from a crystal) GaAs wafer for the photocathode material.

An alternative to the bulk water surface is to grow an additional epitaxial layer, for example, by liquid phase epitaxy, MBE, or MOCVD. Epitaxial layers have fewer defects, leading to diffusion lengths of 3 to 5 μm compared with 0.5 to 1 μm for the bulk wafer. Epitaxial material suitable for photocathodes is not ordinarily available and has to be specially prepared at significant cost.

1.3.2 Surface Cleaning

For optimum activation to NEA, the GaAs surface must be free from contaminants such as C and O. It is possible to get an atomically clean surface by cleaving a (110) crystal, but the cleaving apparatus and the crystal geometry can be cumbersome for source applications. Cleaved (110) surfaces have been tested [51]. There is indication that a lower polarization is obtained from the (110) face [50–52].

If the photocathode is an epitaxial layer grown by MBE, it is possible in the final growth step to lower the temperature of the crystal and expose it to the As_4 beam to grow a protective As layer on the order of 100 nm thick. This protective layer is easily removed by momentarily heating the sample to approximately 400°C a few times. Even with the As protective layer, the photocathode material can oxidize if left in the atmosphere and can degrade in a matter of hours in a particularly humid environment [53]. It is best to store As-capped samples under vacuum to minimize degradation.

The more typical photocathode material, a wafer which has been exposed extensively to atmosphere, requires a chemical cleaning and then heat cleaning in ultrahigh vacuum. The most widely used cleaning procedures employ a mixture of H_2SO_4, H_2O_2, and H_2O with composition ratios in the range of 8 : 1 : 1 to 3 : 1 : 1. A procedure [54] used at SLAC and in our work at NIST employs a 4 : 1 : 1 etch, followed by an etch in concentrated HF and then by a slow etch in a 1 : 1 solution of NaOH and H_2O_2. Details such as the quality of the rinse water and decanting methods are thought to be important. This procedure is described in Appendix A. The aim of the etch is to remove contaminants and form a thin oxide passivation layer before the material is exposed to the atmosphere. Ideally, this layer and any residual contaminants are volatile at temperatures well below temperatures at which As or Ga desorb from the surface.

If it is not possible to put the freshly cleaned photocathode material immediately under vacuum, the surface can be passivated by growing an anodic oxide. The anodization process involves running a current between

the GaAs and a platinum cathode in a phosphoric acid solution as described in detail in Appendix B. The oxide grown is typically 50 to 100 nm thick. The oxide is readily removed by dipping in ammonium hydroxide for about 30 sec. There is some evidence that the anodization and subsequent stripping of the oxide leave a surface which is particularly well suited for the subsequent heat cleaning [53].

The freshly cleaned photocathode is mounted on a sample holder, typically an Mo block, and, ideally, is inserted into a prebaked ultrahigh vacuum chamber through a load lock. In this manner, contamination of the photocathode surface during bakeout is avoided. Nevertheless, adequate photocathodes can be prepared even when the freshly cleaned surface is inserted into the chamber and the chamber is pumped out and then baked. In this case, it is desirable to maintain the photocathode at a temperature approximately 50°C above the typical bakeout temperature of 150 to 200°C.

Once ultrahigh vacuum is attained, impurities at the surface can be desorbed by heating the photocathode to a temperature just below the highest congruent evaporation temperature for free evaporation which is near 660°C for GaAs (100) [55]. Above this temperature, the As evaporates preferentially and leaves behind Ga droplets which give the surface a foggy appearance when viewed with obliquely incident light. Since it is not possible to attach a thermocouple reliably to the GaAs itself, it is best to rely on a relative temperature measurement of an adjacent part and determine the optimum temperature for heat cleaning empirically. This is most easily measured by a using thermocouple mounted in the Mo block on which the GaAs is mounted. An infrared pyrometer can also provide a suitably reproducible measurement of the GaAs temperature.

The apparent temperature for heat cleaning GaAs that gives the best results will vary from one system to another depending on the cathode holder and cathode mounting. One method of determining the optimum heat cleaning temperature, if the cathode can be illuminated and viewed somewhat obliquely, is to heat it to successively higher temperatures, each time allowing it to cool and checking the surface for a frosty appearance. The cathode is sacrificed, but one then knows the correct temperature is 10 to 20°C below that at which the Ga droplets form. Another way to determine the best heat cleaning temperature is to activate the cathode with Cs and O each time after heat cleaning to successively higher temperatures. The quantum efficiency will improve as the heat cleaning temperature is raised to a certain point; above this temperature, the quantum efficiency that can be attained will drop, and one again has determined the optimum heat cleaning temperature. In using this second method, one must be aware that, even when the heat cleaning takes place at the opti-

mum temperature, the subsequent activations are usually better than the first. This may be due to an additional reduction of surface contaminants when a cathode that has already been activated is heat cleaned again. Adequate photocathodes were obtained after heating at the predetermined temperature for as little as 5 min, the whole process of heating and cooling to near room temperature taking less than half an hour [18].

In contrast to the adequate photocathode preparation just described, the optimum photocathode preparation prevents formation of the refractory oxide Ga_2O_3 which is desorbed only at temperatures near the GaAs decomposition temperature. This is accomplished by avoiding any exposure of the chemically cleaned wafer to oxygen or by limiting the exposure to such a degree that less than a monolayer of oxide is formed [53]. In the absence of Ga_2O_3, the heat cleaning can take place at a lower temperature, and as a result there is less surface damage and a correspondingly improved quantum efficiency.

Two approaches to cleaning the GaAs to achieve optimum photocathodes have been reported. In one [53], the chemically cleaned and anodized wafer was mounted with Pt clips and an In bond to the Mo sample holder. The anodization layer was stripped off by immersion in NH_4OH for 30 sec, followed by quick rinses in two beakers of deionized water. The cathode was then blown dry with N_2 and kept under N_2 as it was inserted in the vacuum load lock which was continuously purged with N_2. When this procedure was accomplished quickly, oxygen-free surfaces were obtained after heat cleaning at 500°C [53].

In a second approach [56], the final etch took place in an N_2-filled glove box using a 3 *M* solution of HCl in isopropyl alcohol (ethanol and water were also found to be satisfactory solvents [57]). Provision was made for transferring the sample to the load lock in the N_2 atmosphere to avoid contamination from air. The level of carbon impurities on the GaAs surface was typically 0.4 to 0.6 monolayer, determined to be from residual impurities in the atmosphere of the glove box or load lock. Heating such a surface in ultrahigh vacuum to 400°C reduced the level of carbon impurities to below the detection limit of 0.05 monolayer. It was further shown that when a heavy oxide was intentionally grown on the GaAs surface after introduction into the vacuum but before heat cleaning, the carbon formed a nonvolatile phase which remained on the surface even after heat cleaning to 620°C to remove the oxide [56]. This result is consistent with the general experience, using the usual chemical cleaning methods which also leave an oxide layer, that residual carbon cannot be removed by heating [58].

The key to high quantum efficiency is the avoidance of nonvolatile surface oxides. When this is achieved, the heat cleaning can take place at temperatures at which the surface stoichiometry is not disturbed by

arsenic removal, and the low-temperature heat cleaning is adequate for removing all contaminants including carbon. The possibility of achieving carbon-free surfaces is an important result since there is a direct relationship between quantum efficiency and the residual carbon contamination [58].

1.3.3 Surface Activation

The vacuum level is lowered to achieve NEA by the application of Cs and an oxidant such as oxygen or fluorine (from NF_3). There are a number of ways the activation can take place, and a few of these will now be described. The activation is continuously monitored by measuring the photocurrent, for example, by biasing the anode structure and collecting the emitted electrons. It is worth making the effort to make sure that the light source used during activation can be set up in a reproducible way so that the behavior of one activation can be compared with another.

To monitor the photocurrent, a white light source is desirable because the higher photon energies in the spectrum allow the photocurrent to be monitored well before NEA is achieved. A laser at a photon energy sufficiently above the band-gap energy can also be used to monitor the activation. For comparison with data in the literature, in which photocathode sensitivities are often quoted in μA/L, it is convenient to monitor the activation with a tungsten light source operating at 2856 K which can be calibrated in lumens [55]. A quick check on the response of the cathode to red light is obtained by inserting a filter which transmits light at wavelengths longer than 715 nm. A well-activated cathode typically gives a white-light-to-red-light response ratio of 2 using a 2856 K tungsten light source, whereas this ratio will be higher for a poorly activated cathode. The white-to-red ratio clearly depends on the spectrum of the light source used.

Two sources of Cs are commonly used. The Cs can be obtained by passing a current through a well-outgassed cesium chromate channel as in a commercial Cs dispenser [59]. Alternatively, Cs metal (99.98% pure) is distilled into and sealed in a glass ampoule which can be inserted in a Cu pinch-off tube behind a stainless steel valve [60]. After bakeout, the ampoule is broken by squeezing the Cu tube. For deposition of Cs, the ampoule is maintained at 85 to 90°C. The stainless steel valve which controls the Cs flux is maintained at 150°C so that Cs passes through the open valve without sticking to it [18]. Oxygen or NF_3 is most often let into the cathode region through a leak valve. A heated, thin-walled Ag tube is permeable to oxygen and has also been used to control the oxygen flux [48]. The correct partial pressure of oxygen or NF_3 is determined from the photoresponse. For other pressure measurements, ion gauges

with thoria-coated Ir filaments are used to avoid the CO production that takes place with a hot W filament in the presence of oxygen. However, during activation, it is best to turn off gauges, since any hot filament generates metastable excited oxygen which is more reactive on the GaAs surface and can form undesirable oxides [61].

The heat-treated GaAs surface should be cooled to about 20 to 40°C for activation. Since the Cs and O must have some mobility on the surface to achieve optimum NEA, much lower temperatures are not desirable. The Cs is applied first until the photocurrent reaches a maximum. At this point, one can proceed in a number of ways [55]. One technique is the "yo-yo" technique which is illustrated schematically in Figure 5. After reaching the photocurrent maximum with application of Cs, the Cs is turned off and oxygen is let in until the photocurrent is reduced to about $\frac{1}{3}$ of its previous peak value. The oxygen flow is then stopped, and the Cs is started until a new photocurrent peak is reached, higher than the previous one. After a number of cycles (from about 5 to 20 or more), there is little further increase in photocurrent, and the activation is ended with a slight overcesiation so the peak value decreases by about 10%; the photocurrent will recover a stable equilibrium value. A variation on this procedure is to maintain the Cs flux continuously during the activation and apply the oxygen on and off to peak the photoresponse. The bonding of oxygen to GaAs is greatly enhanced by the presence of a Cs layer; there is some evidence that better activations are obtained if there are two or more monolayers of Cs on the GaAs surface at the time of oxygen exposure [61]. As an alternative to the yo-yo procedure, after the first Cs peak is reached, the Cs can be left on and oxygen admitted concurrently, adjusting the oxygen flow to maximize the rate of increase of photocurrent [18,62]. When there is no further increase in photocurrent, first the oxygen and then the Cs is shut off.

A two-stage activation process has been found to produce about a 30–40% greater quantum efficiency on (100) GaAs surface [62,63]. In this method, the cathode is activated to optimize the sensitivity with a normal yo-yo process as described above and then heat cleaned at a lower temperature in the range 450–550°C. In this second heat cleaning, most of the Cs desorbs, but the oxygen remains. The cathode is then activated a second time to a new higher sensitivity. The higher sensitivity results from a larger NEA and decreased scattering in the activation layer [62].

A fundamental understanding of the Cs–O activation layer is still lacking. The stoichiometry and atomic arrangement of the layer are not known. The activation layer has been modeled as a heterojunction, dipole layer, or cluster system [55,61,62]. There is evidence for an interfacial barrier, shown schematically in Figure 2. Photoemission studies have shown that

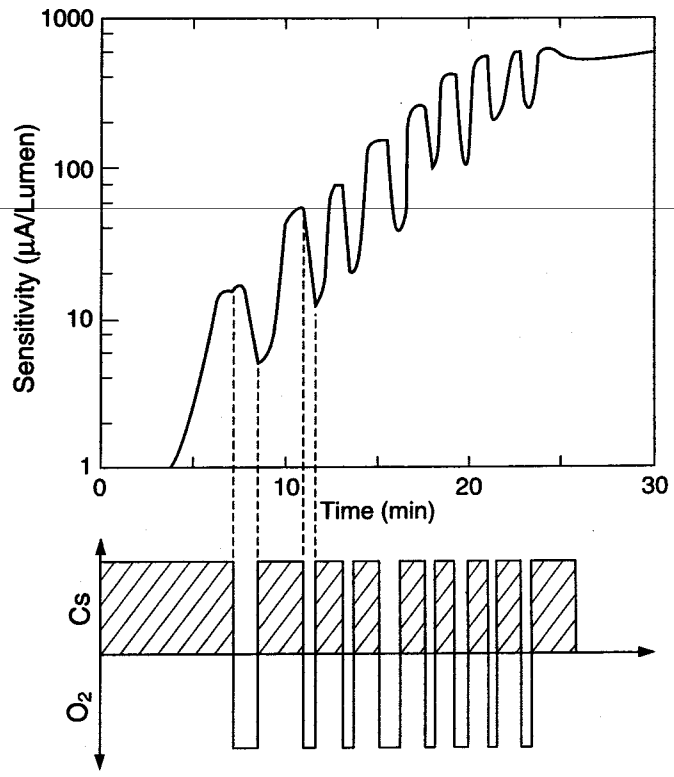

FIG. 5. Schematic of the yo-yo activation of GaAs with alternate cycles of Cs and O_2. A hypothetical but realistic photoresponse curve shows how the sensitivity increases on exposure to Cs and is decreased by O_2 exposure, the cycling of which is indicated at the bottom.

the best activations are achieved when the oxygen goes beneath the Cs to form a GaAs–O dipole layer [61]. This result is consistent with the two-stage activation process, the first stage of which forms a GaAs–O layer, Measurements of the work function at the surface of the activation layer, $E_\infty - E_F$ in Figure 2, showed that the work function continued to decrease with thickness beyond that thickness which gave optimum photoresponse [62]. The escape probability, P_{esc} of Equation (1.2), is increased by a lowering of the vacuum level, but it is decreased by scattering in the activation layer. Although much is not known about the Cs–O layer, it is found experimentally that the final Cs–O stoichiometry is very delicate; changes in either Cs or O of as little as 1–2% can decrease the photoresponse by a factor of 2 [62].

As an alternative to oxygen, NF_3 may be used. It decomposes on the Cs surface, leaving F bonded with the Cs. Because of the larger electronegativity of F compared with that of O, the use of NF_3 might be expected to produce a more stable photocathode. An activation procedure using NF_3 which is a modified yo-yo technique has been developed [35]. After the first peak in photocurrent with exposure to Cs has been obtained, the Cs is turned off and the NF_3 is turned on until a new maximum is reached. The NF_3 is left on and the Cs is turned on until the photocurrent is reduced to about $\frac{1}{3}$ of the previous maximum. The Cs is then turned off and the photocurrent is allowed to reach a new maximum. This process is repeated until there is little change, at which point the Cs is first turned off and then the NF_3 is slowly turned off as the photocurrent reaches a stable maximum. Substantially improved performance using NF_3 has been reported [22], but significant differences in quantum efficiency or lifetime were not observed by some others [48,64].

1.3.4 Quantum Efficiency

The quantum efficiency specifies the quality of the photocathode from the point of view of the current intensity which can be obtained with a given light source. For practical purposes, the definition of the quantum yield as the number of electrons emitted per incident photon is more useful than the yield per absorbed photon which is sometimes quoted. For a known incident light power, p, at wavelength λ, the measured photocurrent gives the yield according to

$$Y = 1.24\, I\ (\mu\text{A})/p\ (\text{mW})\lambda\ (\text{nm}). \qquad (1.5)$$

Thus one obtains 6.45 μA per milliwatt of incident light power at $\lambda = 800$ nm from a GaAs photocathode which has a quantum efficiency of 1%. As a relative measure, some workers quote the yield of GaAs cathodes at the HeNe laser wavelength of 1.96 eV, but this yield can be over a factor of 2 higher than the yield for operation close to threshold. The yield at the operating photon energy is clearly the value of interest.

The yield as a function of photon energy is a useful diagnostic of the photocathode. A small monochromator, such as a 0.25-m Ebert grating monochromator, is adequate for the yield measurement as high resolution by optical standards is not required. A calibrated set of interference filters can also be used. Any of a number of different light sources can be used, such as a halogen lamp, a high-pressure Xe arc lamp, or a Zr arc lamp. At each photon energy, the photocurrent is compared with the incident light power which is easily measured by inserting a commercially available calibrated photodiode into the light beam after the monochromator [18].

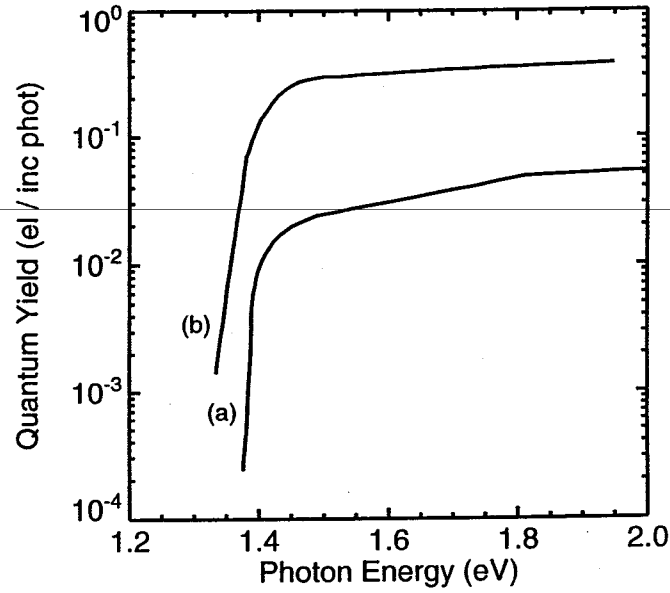

FIG. 6. The quantum efficiency curves of two NEA GaAs(100) reflection photocathodes are compared: (a) adequate photocathode [18] and (b) optimum photocathode [65].

A yield curve from what was described above as an adequate photocathode is compared in Figure 6 with a yield curve from a high-quantum-efficiency optimum photocathode. The adequate photocathode was made from a 5.6- $\times 10^{18}$-cm^{-3} p-type GaAs (100) bulk wafer which was cleaned chemically and by heating [18]. The higher yield curve of Figure 6 was obtained from 7- $\times 10^{18}$-cm^{-3} p-type GaAs (100) grown by vapor-phase epitaxy and activated by the two-stage process [65]. The sharp knee at threshold in the yield curves is characteristic of negative electron affinity. Fitting the yield curves using Equation (1.2) gives $L = 5$ μm and $P_{esc} = 0.55$ for the optimum photocathode [65] and $L = 0.4$ μm and $P_{esc} = 0.1$ for the adequate photocathode [18]. The magnitude of the yield is most sensitive to the escape probability which is much higher for the optimum photocathode presumably because of better cleaning and activation. The quantum efficiency of the optimum photocathode in Figure 6 is unusually high for a reflection photocathode as about 30% of the incident light is reflected. However, such a high-yield curve is typical for commercial transmission cathodes bonded to glass which combine antireflection coatings and the proper GaAs layer thickness to ensure near total absorption of the light [66].

1.3.5 Limitations of the Photocathode Response

When electron pulses are extracted from the photocathode, there are limitations on the minimum duration of the pulses. The photoexcitation process and the thermalization to the conduction band minimum take place rapidly in times on the order of 10^{-15} and 10^{-12} sec, respectively. Even for an arbitrarily short light pulse, the emitted electron distribution is spread in time because of the different transit times for electrons deep inside the active layer and for those near the surface to diffuse to the surface. The shortest electron pulses are obtained for the thinnest active layer, with an accompanying decrease in quantum efficiency. Pulses as short as 8 psec have been observed from an active photoemitting layer estimated to be 50 nm thick [67].

An apparent saturation of the amount of charge in a short, high-intensity electron pulse was observed to occur well below the space-charge limit of the electron gun [68]. The charge per pulse increased linearly with incident photon flux up to a point; beyond this point the charge increased approximately another factor of 2, but more slowly, saturating at a photon flux that was several times higher. This saturation of the photocurrent, that is the "charge limit," varied depending on the quality of activation of a particular cathode. The saturation photocurrent increased with increasing quantum efficiency, but saturated at the same photon flux. Thus the real limit is on the photon flux or light power density. For GaAs doped 2×10^{19} cm^{-3}, the charge per 2-nsec pulse increased linearly up to a power density of approximately 2 kW/cm^2. The nonlinear response is caused by the high light intensities which generate so many electrons that the surface states which determine the band bending become neutralized [69]. When this happens, the vacuum level is shifted higher in energy; this behavior is known as the surface photovoltage or photovoltaic effect. The shift in the vacuum level disappears, and the surface is restored by tunneling and thermionic emission of holes from the valence band into the surface states. For highly doped photocathode material, tunneling from holes into the surface states is the dominant mechanism that restores the surface [69]. Changing the doping of the photocathode from 5×10^{18} to 2×10^{19} cm^{-3} makes the band-bending region narrower, thereby increasing the tunneling probability and the rate at which the photocathode is restored.

In addition to the limit on peak light power density just described, one might expect there to be a limit on the average power density that a cathode could withstand. There have been reports of deterioration of the cathode response at average power densities on the order of 10 W/cm^2 and higher [23]. The mechanism affecting the photoresponse is not clear. It is not a surface photovoltage effect as in the case of high peak power. The heating of the GaAs surface, even assuming that all the light is absorbed at the surface, is calculated to be less than 10°C at this average power density [70]. Experimentally it is known that it is important to avoid contamination of the cathode from gases desorbed if the electron beam hits other surfaces. There needs to be further investigation into the maximum allowable average power density and the mechanism by which it affects the photocathode. As imprecise as these limits on the peak and average light power density are, they are important for estimating the performance of GaAs photocathodes, particularly the maximum brightness.

1.3.6 Photocathode Lifetime

The lifetime of the photocathode is defined as the time taken for the quantum efficiency to fall to $1/e$ of its initial value. Operating photocathode lifetimes vary from minutes to hundreds [48] or even thousands of hours [23]. The activation layer is delicately optimized and any changes in it can cause a decrease in quantum efficiency. One source of contamination is the residual gas in the vacuum chamber which can adsorb onto the photocathode surface and affect both the operating lifetime and the quiescent lifetime, which is analogous to the shelf life of a sealed-off phototube. Another factor limiting the operating lifetime is electron-stimulated desorption of atoms, molecules, or ions from any surfaces hit by the electron beam; desorbed neutrals may drift to the photocathode, but desorbed positive ions can be accelerated to the cathode surface.

An extremely good vacuum in the photocathode region, a pressure of $\leq 10^{-8}$Pa, is desirable. The usual ultrahigh-vacuum precautions regarding cleanliness and materials must be followed. An ion pump, possibly supplemented by a nonevaporable getter pump, can be used for pumping. The electron gun anode structure and subsequent electron optics must be carefully designed so that the electron beam does not strike their surfaces. If the polarized electron source must be attached to an apparatus with a poorer vacuum, differential pumping between the source and the apparatus can be employed [71].

The detailed mechanism at the photocathode surface which causes the decay in quantum efficiency is not well understood and, in fact, may be different in different situations. When the quantum efficiency has decreased, it is usually found that the photocathode is Cs deficient. Whether this is because an oxidant has adsorbed on the surface or because Cs has left the surface is not usually known. The photocathode efficiency, however, can be restored by addition of Cs. In sealed-off phototubes, there is a built-in excess of Cs which maintains cathode equilibrium and avoids a decrease in the quantum efficiency. In an ultrahigh-vacuum cham-

ber, lifetimes are usually found to increase after a few activations, when the region around the photocathode becomes coated with Cs. In low-energy electron-gun applications, it is possible for the cathode to be continuously cesiated at a low rate to achieve very long lifetimes [72]. This treatment may not be possible in accelerator applications in which continuous cesiation may cause unwanted field emission from parts of the cathode structure at high voltage.

1.4 Incident Radiation

The photon energy of the photoexciting radiation should be within about 0.1 eV of the band-gap energy (much closer for strained layer cathodes). The incident photon intensity may be continuous or pulsed (subject to the limits on peak power density discussed above). Some examples of the many different kinds of lasers that have been used are an AlGaAs diode laser [18,73], an HeNe laser [46,73], a flash-pumped dye laser [19,48], and a YAG-pumped pulsed Ti : sapphire laser [74]. Because of the rapid photocurrent response time of GaAs photocathodes, it is possible to obtain current pulses with a wide variety of shapes by controlling the intensity of the incident radiation. For some accelerator applications, the photocurrent is sensed and a feedback system controls the light intensity during a pulse to obtain the required rectangular shape [48].

The light is circularly polarized using a linear polarizer, such as a Glan–Thompson prism, followed by a quarter-wave retarding element, such as a Pockels cell or quarter-wave plate as illustrated in Figure 7. When the quarter-wave voltage of the Pockels cell is reversed, the fast axis in Figure 7 becomes a slow axis and the photon helicity reverses from positive to negative. The degree of polarization can be measured using a photodiode and a second linear polarizer, crossed with the first, to detect the light passing through the Pockels cell. By measuring the maximum intensity I_{max} and minimum intensity I_{min} when the Pockels cell voltage is reversed, the degree of circular polarization P_{CP} can be found,

$$P_{CP} = 2(I_{max}I_{min})^{1/2}/(I_{max} + I_{min}), \qquad (1.6)$$

where the approximation has been made that the linear polarizers are perfect [75].

Very sensitive measurements of spin-dependent processes are achieved by detecting an experimental signal synchronously with the switching of the incident electron beam polarization. When small experimental asymmetries are to be measured, the electron beam polarization can be reversed

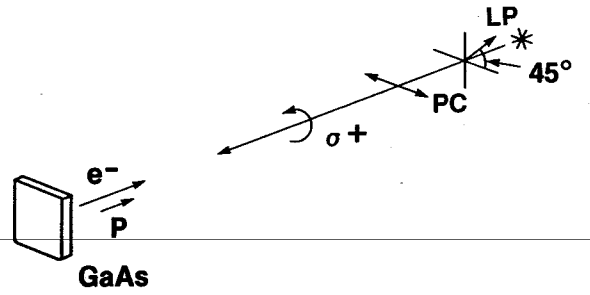

FIG. 7. The arrangement of optical elements to produce a particular electron spin polarization. Light from a source (*) passes through a linear polarizer (LP) defining the plane of vibration of the electric vector at 45° to the fast axis (for the electric vector) of a Pockels cell (PC). The electric vector of the resultant circularly polarized light, as observed at a fixed point on the light axis, moves in the direction of the curved arrow. This is called σ^+ light and corresponds to the light angular momentum in the direction of light propagation. The spin polarization of electrons emitted from the GaAs is antiparallel to the incident light angular momentum.

rapidly and randomly on a pulse-to-pulse basis to minimize the affect of drift or possible switching of the beam polarization synchronously with other experimental parameters [20]. High sensitivity is achieved only if instrumental asymmetries, such as changes in the beam phase space or beam current when the polarization is reversed, are minimized. The instrumental asymmetry is defined as, $A = (I^+ - I^-)/(I^+ + I^-)$, where I^+ (I^-) is the current emitted for photoexcitation with σ^+ (σ^-) light. When extreme care is taken to align the Pockels cell, adjust the Pockels cell voltages, and compensate any birefringence of the vacuum windows, instrumental asymmetries as small as 6×10^{-6} can be achieved [48].

The energy spread of the electron beam from GaAs was observed to increase to as much as several electron volts when particular lasers were used to excite the photoelectrons [73]. This result was quite unexpected since most previous measurements found the energy spread ΔE in the range of 100 to 200 meV and under particular conditions as low as 30 meV [46,76,77]. This broadening was observed for excitation with intense HeNe lasers but not with diode lasers. It was attributed to very rapid fluctuations which result from interferences between the many modes of these lasers [73]. The apparently constant laser intensity actually consists of many rapid short pulses that give rise to intense bunches of emitted electrons that result in an energy broadening [78]. Clearly, the laser used to photoexcite the electrons must be carefully selected when the energy spread of the beam is a consideration.

1.5 Operation of the Photocathode in an Electron Gun

Certain electron optical parameters of the photocathode determine what the optimum performance can be in a particular application. These are estimated for NEA GaAs and compared with measurements of actual GaAs photocathode performance and with the performance of other electron sources. Two examples are given of the wide variety of electron guns which have GaAs photocathodes.

1.5.1 Electron-Optical Considerations

The electron-optical phase-space volume of the emitted electron beam determines the fraction of the beam that can be accepted by the device to which the electron gun is coupled. A useful description of the beam is given by the product of the electron beam energy, E; the cross-sectional area, dA; and solid angle, $d\Omega$. The product is conserved according to the law of Helmholtz and Lagrange [79]. In the paraxial ray approximation this law leads to $E_1A_1\Omega_1 = E_2A_2\Omega_2$ for any two points, 1 and 2, along the beam, assuming conservation of current I. This conserved quantity is related to the concept of emittance which is used to describe electron beam quality. The emittance ε is defined as $1/\pi$ times the area in transverse phase space at a point along the beam. In the paraxial ray approximation, $\varepsilon = RR'$ for an axially symmetric beam, where R is the radius of the electron beam at the source or an image of the source and R' is the cone half-angle at that point. The quantity $\varepsilon E^{1/2}$ is sometimes referred to as the emittance invariant ε_{inv}, since $EA\Omega = (\pi\varepsilon_{inv})^2$. The emittance is readily generalized to nonaxially symmetric situations as well as to the relativistic case, in which the emittance invariant is written [80] $\varepsilon_{inv} = \beta\gamma\varepsilon$, where $\beta = v/c$, the electron velocity relative to the speed of light, and $\gamma = (1 - \beta^2)^{-1/2}$. Another quantity used to characterize the electron beam is the brightness, defined as the current per unit area per unit solid angle, $B = dI/dAd\Omega$. From the law of Helmholtz and Lagrange, it is seen that B/E is a conserved quantity and is known as the invariant brightness. In the relativistic limit the invariant brightness is written $B/\beta^2\gamma^2$. These relations show that the maximum current which can be incident at energy E onto a target in area dA and solid angle $d\Omega$ is determined by the invariant brightness B/E.

The emittance and brightness describe the GaAs photocathode for electron optical design purposes. Possible nonlinearities, aberrations, and space-charge effects can distort the emittance phase space and reduce the effective brightness in actual electron-optical systems. However, it is useful to estimate the photocathode brightness to obtain an upper limit.

In the absence of scattering in the band-bending region or at the surface, the angular spread of the photoemitted electrons is determined by the conservation of parallel wave vector and the ratio of the effective mass of an electron in the conduction band to the free-electron effective mass. For this ideal situation, Bell [28] calculated a minimum emission cone half-angle of $\alpha = 4°$ at room temperature. A larger value, $\alpha = 12°$, was measured [81] and attributed to roughness of the cathode surface. However, transverse energies of the photoelectrons of 40 to 100 meV corresponding to cone half-angles of approximately 25° to 30° have been measured and attributed to additional scattering, possibly in the activation layer [62,66,82]. The brightness can be written, $B = J/\pi\alpha^2$, where J is the current density. Using the measured $\alpha = 12°$ and an average electron emission energy of 0.2 eV, we arrive at an expression for the invariant brightness $B/E = 36J$ (A/cm^2-sr-eV), which would of course be decreased if a larger emission cone is assumed.

1.5.2 Performance

Some upper limits on the brightness can be estimated, taking the maximum average and peak light power densities of 10 W/cm^2 and 2 kW/cm^2, respectively, and a quantum efficiency of 0.3. The corresponding current densities are approximately 2 and 400 A/cm^2, from which we obtain values of the invariant brightness of 0.7×10^2 and 1.4×10^4 A/cm^2-sr-eV, respectively. In the pulsed mode, current densities of 180 A/cm^2 have been reported [83]. When a GaAs photocathode was used as the cathode in a scanning electron microscope, the electron beam brightness in the continuous mode at 3 keV was measured [81,84] to be 1×10^5 A/cm^2-sr. Measurements were made with the same average current in the pulsed mode with a duty cycle of 0.8%, leading to a pulsed brightness of 1.2×10^7 A/cm^2-sr. These measured brightness values can be compared with the 3-keV values of 2.1×10^5 and 4.2×10^7 A/cm^2-sr calculated from the continuous and pulsed invariant-brightness estimates, respectively.

Using the relativistic form of the invariant brightness, we calculate brightness values of 3.6×10^6 and 4.8×10^8 A/cm^2-sr at 100 keV, for the continuous and pulsed modes, respectively, from the measured brightness values at 3 keV. The 3-keV brightness values were not measured under optimum conditions, and further measurements are required to determine whether higher values can be attained [84]. These GaAs photocathode brightness values at 100 keV are compared in Table I with typical values [85] for LaB_6, a W hairpin filament, a pointed W filament, and heated field emission sources. The brightness of NEA GaAs in the continuous mode is about 10 times that of the W hairpin filament and approximately

TABLE I. NEA GaAs Compared with Sources of Unpolarized Electrons

Source	Brightness at 100 keV (A cm^{-2} sr^{-1})	ΔE FWHM (eV)
NEA GaAs		
Continuous	3.6×10^6	0.1–0.2
Pulsed	4.4×10^8	
LaB_6	7×10^6	1
W hairpin filament	5×10^5	0.7–2.4
Pointed W filament	2×10^6	2
Heated field emission	10^7–10^8	0.3

comparable to that of LaB_6. For pulsed applications, the brightness of NEA GaAs is much higher than that of LaB_6 and even higher than that of heated field emission sources.

The energy spread and vacuum requirements of the electron sources in Table I are quite varied. The LaB_6 and W cathodes operate at 1300–1500 and 2300–2500°C, respectively, leading to a fairly high energy spread of the emitted beams as noted in Table I. The electron affinity of a GaAs cathode can be adjusted to obtain an energy spread as narrow as 30 meV, but with much lower quantum efficiency. Values of $\Delta E = 0.1$–0.2 eV are estimated for GaAs operating in the high-brightness continuous mode. Somewhat larger values of ΔE can occur in systems with larger NEA or, in the case of reflection photocathodes, when the photon energy is significantly larger than the band gap and when nonthermalized electrons form a substantial part of the photoelectron energy distribution. There is evidence for further broadening in the pulsed mode [81], possible related to the broadening discussed in Section 1.4; additional investigation of this effect is needed. Thus, it may be possible to attain a factor of 2 or so lower ΔE values from NEA GaAs than from the heated field emitter; if attainable, such cathodes would be a significant improvement for low-energy electron microscopy applications. The field-emission and GaAs cathodes require ultrahigh vacuum, whereas the W and LaB_6 require only a moderate vacuum, a pressure of 10^{-3} Pa or lower.

The noise properties and stability of GaAs cathodes have been measured [84]. When a stabilization-feedback loop diminished the laser noise, the noise spectrum was found to be near the shot-noise limit. By measuring the emitted current on a spray aperture and controlling the laser power, the drift in a 3-hr period was less than 0.04%. The emission from the cathode as observed on a phosphor screen was found to be uniform without hot spots [81].

1.5.3 Examples of Polarized Electron Guns

Many electron-optical systems have been used with GaAs cathodes. The applications vary from a low-energy electron diffraction (LEED) gun [18] to a pulsed scanning electron microscope [84] and the injector for a linear accelerator [19]. For the low-energy applications, space-charge considerations dominate before brightness limits are reached. In higher energy applications, such as electron microscopy, guns are brightness limited. Electron guns employing GaAs photocathodes have generally used a simple diode configuration consisting of the photocathode and an anode. The triode configuration, in which a control electrode between the cathode and the anode forms a crossover, was ruled out for pulsed electron microscopy because of the space-charge-induced electron energy spread in the crossover [81].

The original SLAC GaAs-polarized electron gun [19] used for the parity-violation experiments [20,21] is shown in Figure 8. This gun, which has been a model for a number of later guns for accelerator applications, is very similar to thermionic guns used on SLAC, the main difference being the use of the GaAs photocathode instead of a thermionic emitter. The cathode geometry is shaped to optimize space-charge-limited operation, and the anode, as with the subsequent electron optics, is designed so as not to intercept any electrons which would desorb gases and limit the cathode lifetime as discussed in Section 1.3.6. The large insulator allows cathode operation at −70 keV as required for injection into the accelerator. Since the time of these experiments, it has been found that good results can be obtained without cooling the cathode or surrounding regions.

An example of a low-energy polarized electron gun is shown in Figure 9. For this type of application, the anode is simply a flat plate with a hole in it. When space charge is a limitation, it usually occurs when the beam is focused at low energy downstream in the electron optics. The anode is followed by a 90° spherical deflector which deflects the electron beam from the path of the incident laser radiation. The spherical deflector also acts as a focusing element. According to Barber's rule, the object (actually the virtual object which in this case is 3 mm behind the GaAs surface), the center of curvature of the deflector, and the image lie on a straight line. Two sets of deflection plates capable of changing the beam angle or laterally shifting the beam precede the acceleration to 1000 eV. Up to this point, labeled X in Figure 9, this polarized electron gun is fairly generic, while beyond this point it is designed to be a LEED gun as shown in the lower part of the figure. Alternatively, it could be designed to produce a lower energy and higher current beam as required for inverse photoemis-

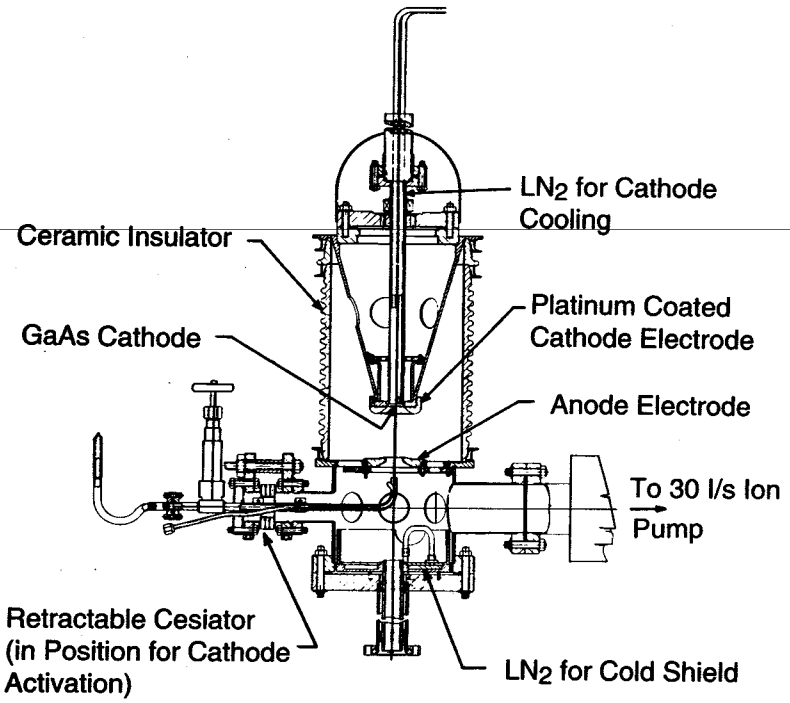

FIG. 8. Schematic of the initial SLAC GaAs polarized electron gun developed for the parity violation experiment. The cathode is at a potential of −70 kV, suitable for injection into the linear accelerator. From Sinclair [19].

sion [73]. The lens elements of this LEED gun were made of Cu, whereas those of the inverse photoemission gun [73] were made of Al and were coated on the inside with a graphite layer. In each case, care was taken to ensure that there was no line of sight from the electron beam to the insulators separating the electrodes. Molybdenum is a suitable material for the apertures.

1.5.4 Spin Rotation

The electron beam extracted from the GaAs photocathode is longitudinally polarized; that is, the axis of electron spin polarization is along the electron momentum. For most low-energy condensed matter experiments, a transverse polarization is desired. This objective is accomplished in the source shown in Figure 9 by the transverse electric field of the 90° electrostatic deflector which, at nonrelativistic energies, changes the beam

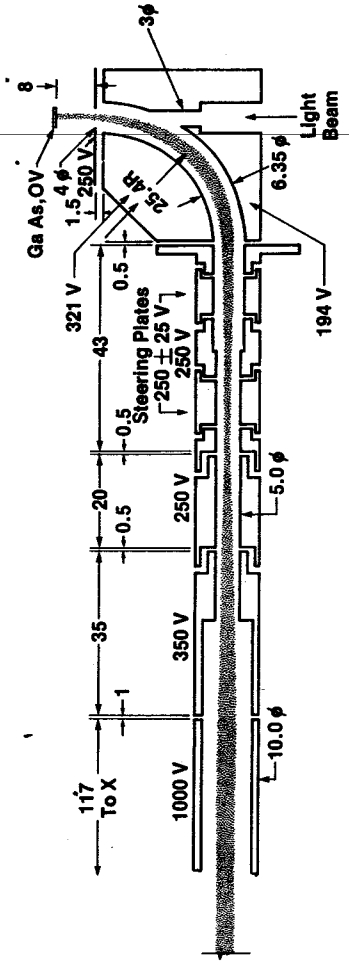

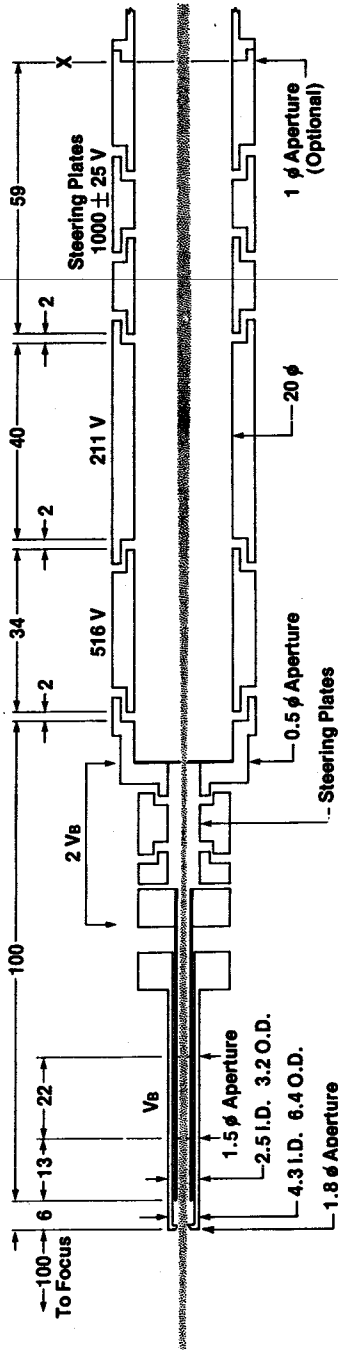

FIG. 9. Schematic of the low-energy polarized electron gun developed at NIST. The upper part of the figure is a generic polarized electron source. The light is incident through a hole in the 90° spherical deflector that deflects the beam to the electron optics that transport the electrons to the vacuum isolation valve. The lower part of the figure shows the electron optics which follow the valve and are specialized for a LEED gun. The calculated beam envelope is shown from the photocathode to the target. From Pierce *et al.* [18].

direction without changing the spin direction. At high energies, relativistic corrections are required [86]. For example, an electrostatic deflector with a bending angle of 107.7° is required to rotate the spin of a 100-keV beam by 90°. For a transverse magnetic field, the spin polarization direction follows the electron momentum in the nonrelativistic limit.

In most high-energy experiments, a longitudinal polarization is required at the scattering target. Magnetic fields in accelerators can cause the spin direction of the relativistic electrons to change during transport. It is desirable to be able to adjust the polarization direction of the beam relative to the electron momentum at the source in order to achieve the desired longitudinal polarization at the target for each energy. An elegant system, employing two electrostatic deflectors and two systems of solenoids each consisting of two double solenoids, that allows the selection of the spin direction of 100-keV electrons to be in any direction before injection into the accelerator has been described [87,88]. This spin rotator has the advantage that the electron-optical properties of the beam are otherwise unchanged.

1.6 Summary

A number of different polarized electron sources are compared in Table II, which is an updated version of previous comparisons [1,2,16,18]. There are significant changes in the entries for the NEA GaAs and flowing He afterglow sources, but there has not been further development of the other types of spin-polarized sources which are included for comparison. The optimum source for a particular application depends on a number of interrelated factors. For some, a minimum asymmetry on switching the electron beam polarization may be most important, whereas for others the highest polarization or the time structure of the beam is the overriding factor.

The developments in GaAs-type polarized electron sources are listed in the first part of Table II. For this type of source an extra column, the quantum efficiency, is included since the beam current is determined, within the limits discussed previously, by the incident radiation. Only published values of polarization and quantum efficiency are listed. The strained layer and superlattice cathodes are undergoing continuous improvement. Significant increases in the figure of merit P^2I can be expected, largely as a result of increases in the quantum efficiency without polarization reduction. The peak pulsed current listed is typical for SLAC [68]. The smallest energy spreads are attained by adjusting the vacuum level with a corresponding decrease in quantum efficiency. Energy spreads greater that 0.3 eV have been reported at higher photon energies, for

TABLE II. Comparison of Spin-Polarized Electron Sources

Method		P	Reversal of P	I_{de}	I_{pulse} (el/pulse) (rep. rate)	ΔE (eV)	$EA\Omega$ (eV cm^2 sr)
Photoemission from			Optical				2.2×10^{-8}
NEA GaAs (100)	QE						
Bulk GaAs						0.03–0.3	
"Adequate" [18]	3×10^{-2}	0.25–0.4		20 μA/mW[a]			
"optimum"	3×10^{-1}			200 μA/mW[a]	10^{11}/2 nsec 120 Hz		
Thin (0.2 μm) GaAs [32]	1×10^{-2}	0.49					
GaAs/GaP$_x$As$_{1-x}$							
[40]	8×10^{-4}	0.83					
[41]	4×10^{-4}	0.90					
[41]	1×10^{-3}	0.80					
Superlattice [43]	3×10^{-6}	0.71		1 μA		0.15–0.4	$<4.3 \times 10^{-2}$
Optically pumped flowing		0.80	Optical	10 μA			
He afterglow [11]		0.75					
Photoemission from EuO [7]		0.61	Magnetic field	1 μA	3×10^9/1.5 μsec	2	1.8×10^3
Field emission from W–EuS [6]		0.85	Magnetic field	0.01 μA		0.1	10^{-11}
Fano effect							
Rb [4]		0.65	Optical		2.2×10^9/12 nsec 50 Hz	<500	1.1
Cs [5]		0.63		0.01 μA		3	3.9
Photoionization polarized Li [3]		0.85	Magnetic field		2.2×10^9/1.5 μsec 180 Hz	1500	<64

[a] The maximum current is determined by light power subject to limitations described in the text.

photocathodes such as GaAsP which have a larger NEA, and for some pathological cases mentioned in Sections 1.4 and 1.5.2. A beam energy spread of 0.1 to 0.2 eV is typical in ordinary operation. The energy-area-angle phase-space product for the GaAs source is calculated assuming an initial energy of 0.2 eV and an area corresponding to a 10-μm-diameter light spot which can be attained with ordinary optics. Using the emission cone half-angle of 12°, one calculates $EA\Omega = 2.2 \times 10^{-8}$ eV-cm^2-sr. This small value, which obviously depends on the assumed values, gives flexibility in the electron-optical design.

The optically pumped, flowing-He-afterglow polarized electron source has undergone further development which produced the significantly improved results listed in the second entry of Table II. This source also uses optical pumping, in this case of the metastable He(2^3S) in the flowing He afterglow generated by a microwave discharge. Using circularly polarized $2^3S \rightarrow 2^3P$ radiation one spin state is preferentially populated. When a target gas such as CO_2 is injected into the afterglow, spin conserving chemionization reactions take place, resulting in polarized electrons that can be extracted from the afterglow region and formed into a beam. Like the GaAs source, the spin polarization is conveniently reversed by reversing the circular polarization of the light. The absence of the need for ultrahigh vacuum is an advantage of the flowing He afterglow source for some applications. High polarizations of 0.80 and 0.75 at beam currents of 1 and 10 μA, respectively, have been achieved [11].

Cardman [89] compared various NEA GaAs sources and the flowing He afterglow source for three accelerator experiments: the low-current polarized target and higher current parity-violation experiments at the Continuous Electron Beam Accelerator Facility (CEBAF) and the Z^0 experiment at the Stanford Linear Collider (SLC). The high polarization that can be obtained at low currents from the flowing He afterglow source makes it competitive with the strained layer GaAs source for polarized target experiments at CEBAF [89]. The strained-layer GaAs/GaP_xAs_{1-x} source parameters are superior for the high-current CEBAF experiments and the pulsed SLC experiments.

In addition to its wide application as a source of spin-polarized electrons for particle, atomic, and condensed matter physics [90], the NEA GaAs photocathode makes possible the coupling of high-speed laser technology and electron-beam instrumentation in applications for which electron spin may be of no concern, such as time-resolved electron microscopy and spectroscopy. This feature, coupled with the high brightness of these photocathodes and small energy spread, presents many opportunities for fruitful application of NEA GaAs photocathodes.

Acknowledgments

Many helpful discussions with numerous colleagues at NIST and elsewhere are gratefully acknowledged. This work was supported in part by the Office of Naval Research.

Appendix A: Cleaning GaAs

The following procedure for cleaning GaAs (adapted from Pierce *et al.* [18]) is one of a number of procedures which have been reported. Important factors are thought to be using deionized water with a resistivity of >15 MΩ-cm, using electronic-grade chemicals and fresh etching solutions, and concluding etch steps (7,10,12) by flushing GaAs with deionized water without exposing it to air.

1. Ultrasonically clean four polyethylene beakers, Teflon tweezers, and a graduated cylinder in 1,1,1-trichloroethane, acetone, and methanol.
2. Prepare a 4 : 1 : 1 mixture of concentrated H_2SO_4, 30% H_2O_2, and H_2O by volume. Carefully add the H_2SO_4 to the H_2O_2 and H_2O to avoid heating above 80°C.
3. Prepare a 1 : 1 mixture of NaOH (1 *M* solution, 4 g NaOH to 100 ml H_2O) and H_2O_2 (0.76 *M* solution, 1 ml 30% H_2O_2 to 11.5 ml H_2O).
4. Ultrasonically clean the crystal at low power in trichloroethane for 3 min. Decant trichloroethane leaving the GaAs slightly covered. Add new trichloroethane and repeat this step two more times.
5. Decant the trichloroethane and rinse the crystal with methanol, decanting off the liquid leaving the GaAs slightly covered. Repeat this methanol rinse two more times. Ultrasonically clean the crystal at low power in methanol for 3 min. Decant the methanol leaving the crystal slightly covered. Add fresh methanol and repeat the ultrasonic step two more times.
6. Blow dry the crystal with filtered dry N_2.
7. Etch the crystal in the 4 : 1 : 1 mixture at 50°C for 3 min, face up. Agitate the solution to keep fresh etch at the surface.
8. Rinse the crystal in 10 changes of deionized water always keeping it covered by some water. Rinse the crystal in 6 changes of methanol, again always keeping the crystal covered with some of the liquid.
9. Blow dry the crystal with filtered dry N_2 and make a visual inspection at this point. If the crystal is not clean and shiny, start over with a new crystal.

10. Etch the crystal face up in undiluted (48%) HF, agitating the solution for 5 min at room temperature.
11. Rinse the crystal twice in deionized water.
12. Etch the crystal in 1 : 1 solution (from step 3) for 1 min at room temperature.
13. Rinse the crystal five times in deionized water keeping the crystal surface covered. Rinse five times in methanol again keeping the surface covered. Blow the crystal dry with filtered dry N_2 and install it in the vacuum system immediately.

Appendix B: Anodization of GaAs

The following procedure [91] is adapted from Schwartz *et al.* [92].

1. Prepare a 2.5 pH phosphoric acid (H_3PO_4) solution by adding two to three drops of 85% H_3PO_4 phosphoric acid to 800 ml deionized water.
2. Form a loop, about 2 cm in diameter, from 0.05-mm-diameter Pt wire for the cathode. Suspend it from the edge of a clean 100-ml beaker so it is about 1 cm from the bottom.
3. Sheath the ends of stainless steel tweezers with pure Al so that no metals other than Pt and Al contact the anodizing solution.
4. Add the anodizing solution to the beaker. Before using the sheathed tweezers to hold the GaAs, anodize the tips by applying −50 V to the Pt wire and wait until the current stabilizes. The disturbance of GaAs anodization is minimized by preanodizing the tweezers.
5. Remove the tweezers and scrape off a bit of the anodization for good electrical contact with the GaAs chip.
6. Hold the GaAs in the tweezers face up under the Pt loop in fresh anodizing solution. The GaAs can be transferred directly from the deionized water rinse of cleaning step 13 (Appendix A) to the anodizing solution.
7. Apply −40 to −50 V DC to the Pt wire to begin anodization. Monitor the current and continue anodization until it stabilizes at its minimum value for 1 min; bubbles will cease to form on the surface.
8. Remove the GaAs and rinse it in five changes of deionized water and methanol. Blow dry the GaAs with filtered dry N_2.
9. The anodization layer can be removed by agitating it face up in 30% NH_4OH for 30 sec. Rinse the GaAs with 10 changes of deionized water without exposing it to air. Blow dry the GaAs with N_2 and install it immediately in a vacuum system (preferably maintaining the GaAs under an N_2 atmosphere [53]).

References

1. J. Kessler, *Polarized Electrons*. Springer-Verlag, Berlin, 1985.
2. R. J. Celotta and D. T. Pierce, *Adv. At. Mol. Phys.* **16,** 101 (1980).
3. M. J. Alguard, J. E. Clendenin, R. D. Ehrlich, V. W. Hughes, J. S. Ladish, M. S. Lubell, K. P. Schüler, G. Baum, W. Raith, R. H. Miller, and W. Lysenko, *Nucl. Instrum. Methods* **163,** 29 (1979).
4. W. von Drachenfels, U. T. Koch, T. M. Müller, W. Paul, and H. R. Schaefer, *Nucl. Instrum. Methods* **140,** 47 (1977).
5. P. F. Wainwright, M. J. Alguard, G. Baum, and M. S. Lubell, *Rev. Sci. Instrum.* **49,** 571 (1978).
6. E. Kisker, G. Baum, A. H. Mahan, W. Raith, and B. Reihl, *Phys. Rev. B* **18,** 2256 (1978).
7. E. Garwin, F. Meier, D. T. Pierce, K. Sattler, and H. C. Siegmann, *Nucl. Instrum. Methods* **120,** 483 (1974).
8. P. J. Keliher, R. E. Gleason, and G. K. Walters, *Phys. Rev. A* **11,** 1279 (1975).
9. L. A. Hodge, F. B. Dunning, and G. K. Walters, *Rev. Sci. Instrum.* **50,** 1 (1979).
10. L. G. Gray, K. W. Giberson, C. Cheng, R. S. Keiffer, F. B. Dunning, and G. K. Walters, *Rev. Sci. Instrum.* **54,** 271 (1983).
11. G. H. Rutherford, J. M. Ratliff, J. G. Lynn, F. B. Dunning, and G. K. Walters, *Rev. Sci. Instrum.* **61,** 1460 (1990).
12. E. Garwin, D. T. Pierce, and H. C. Siegmann, *Helv. Phys. Acta* **47,** 393 (1974).
13. G. Lampel and C. Weisbuch, *Solid State Commun.* **16,** 877 (1975).
14. D. T. Pierce, F. Meier, and P. Zürcher, *Phys. Lett. A* **51A,** 465 (1975).
15. D. T. Pierce, F. Meier, and P. Zürcher, *Appl. Phys. Lett.* **26,** 670 (1975).
16. D. T. Pierce and F. Meier, *Phys. Rev. B* **13,** 5484 (1976).
17. D. T. Pierce, F. Meier, and H. C. Siegmann, U. S. Pat. 3,968,376 (1976).
18. D. T. Pierce, R. J. Celotta, G.-C. Wang, W. N. Unertl, A. Galejs, C. E. Kuyatt, and S. R. Mielczarek, *Rev. Sci. Instrum.* **51,** 478 (1980).
19. C. K. Sinclair, *AIP Conf. Proc.* **35,** 426 (1976).
20. C. Y. Prescott, W. B. Atwood, R. L. A. Cottrell, H. DeStaebler, E. L. Garwin, A. Gonidec, R. H. Miller, L. S. Rochester, T. Sato, F. J. Sherden, C. K. Sinclair, S. Stein, R. E. Taylor, J. E. Clendenin, V. W. Hughes, N. Sasao, K. P. Schüler, M. G. Borghini, K. Lübelsmeyer, and W. Jentschke, *Phys. Lett. B* **77B,** 347 (1978).
21. C. Y. Prescott, W. B. Atwood, R. L. A. Cottrell, H. DeStaebler, E. L. Garwin, A. Gonidec, R. H. Miller, L. S. Rochester, T. Sato, F. J. Sherden, C. K. Sinclair, S. Stein, R. E. Taylor, C. Young, J. E. Clendenin, V. W. Hughes, N. Sasao, K. P. Schüler, M. G. Borghini, K. Lübelsmeyer, and W. Jentschke, *Phys. Lett. B* **84B,** 524 (1979).
22. C. K. Sinclair, *Proc. Int. Symp. High Energy Spin Phys. 6th*, Marseille, *1984; J. Phys.* **46,** C2-669 (1985).
23. C. K. Sinclair, *Proc. Int. Symp. High Energy Spin Phys. 8th*, Minneapolis, *1988; AIP Conf. Proc.* **187,** 1412 (1989).
24. E. Reichert, *Proc. Int. Symp. High Energy Spin Phys. 9th*, Bonn, *1990*, Vol. 1, p. 303 (1991).
25. T. Nakanishi, *Proc. Int. Symp. High Energy Spin Phys. 10th*, Nagoya, *1992*. p. 279–290. (Universal Academy Press Inc., Tokyo).

26. W. E. Spicer, *Phys. Rev.* **112,** 114 (1958).
27. W. E. Spicer, *Appl. Phys.* **12,** 115 (1977).
28. R. L. Bell, "Negative Electron Affinity Devices." Oxford Univ. Press (Clarendon), Oxford, 1973.
29. L. W. James and J. L. Moll, *Phys. Rev.* **183,** 740 (1969).
30. G. Fishman and G. Lampel, *Phys. Rev. B* **16,** 820 (1977).
31. G. Lampel and M. Eminyan, *Proc. Int. Conf. Phys. Semiconduct. 15th, 1980; J. Phys. Soc. Jpn.* **49,** Suppl. A, 627 (1980).
32. T. Maruyama, R. Prepost, E. L. Garwin, C. K. Sinclair, B. Dunham, and S. Kalem, *Appl. Phys. Lett.* **55,** 1686 (1989).
33. P. Zürcher and F. Meier, *J. Appl. Phys.* **50,** 3687 (1979).
34. F. Meier, A. Vaterlaus, F. P. Baumgartner, M. Lux-Steiner, G. Doell, and E. Bucher, *Proc. Int. Symp. High Energy Spin Phys. 9th,* Bonn, *1990,* Vol. 2, p. 25 (1991).
35. B. M. Dunham, Ph.D. Thesis, University of Illinois, Urbana (1993).
36. T. Maruyama, E. L. Garwin, G. H. Zapalac, J. S. Smith, and J. D. Walker, *Phys. Rev. Lett.* **66,** 2376 (1991).
37. J. W. Matthews and A. E. Blakeslee, *J. Cryst. Growth* **27,** 118 (1974).
38. P. J. Orders and B. F. Usher, *Appl. Phys. Lett.* **50,** 980 (1987).
39. T. Nakanishi, H. Aoyagi, H. Horinaka, Y. Kamiya, T. Kato, S. Nakamura, T. Saka, and M. Tsubata, *Phys. Lett. A* **158A,** 345 (1991).
40. H. Aoyagi, H. Horinaka, Y. Kamiya, T. Kato, T. Kosugoh, S. Nakamura, T. Nakanishi, S. Okumi, T. Saka, M. Tawada, and M. Tsubata, *Phys. Lett. A* **167A,** 415 (1992).
41. T. Maruyama, E. L. Garwin, R. Prepost, and G. H. Zapalac, *Phys. Rev. B* **46,** 4261 (1992).
42a. T. Saka, T. Kato, T. Nakanishi, M. Tsubata, K. Kishino, H. Horinaka, Y. Kamiya, S. Okumi, C. Takahashi, Y. Tanimoto, M. Tawada, K. Togawa, H. Aoyagi, and S. Nakamura, *Jpn. J. Appl. Phys.* **32,** L1837 (1993).
42b. J. C. Gröbli, D. Oberli, F. Meier, A. Dommann, Yu. Mamaev, A. Subashiev, Yu. Yashin, *Phys. Rev. Lett.* **74,** 2106 (1995).
43. T. Omori, Y. Kurihara, T. Nakanishi, H. Aoyagi, T. Baba, T. Furuya, K. Itoga, M. Mizuta, S. Nakamura, Y. Takeuchi, M. Tsubata, and M. Yoshioka, *Phys. Rev. Lett.* **67,** 3294 (1991).
44. T. Nakanishi, Nagoya University, private communication Feb. 15, 1994.
45. C. Conrath, T. Heindorff, A. Hermanni, N. Ludwig, and E. Reichert, *Appl. Phys.* **20,** 155 (1979); E. Reichert and K. Zähringer, *Appl. Phys. [Part] A* **A29,** 191 (1982).
46. J. Kirschner, H. P. Oepen, and H. Ibach, *Appl. Phys. [Part] A* **A30,** 177 (1983).
47. F. Ciccacci, S. F. Alvarado, and S. Valeri, *J. Appl. Phys.* **53,** 4395 (1982).
48. W. Hartmann, D. Conrath, W. Gasteyer, H. J. Gessinger, W. Heil, H. Kessler, L. Koch, E. Reichert, H. G. Andresen, T. Kettner, B. Wagner, J. Ahrens, J. Jethwa, and F. P. Schäfer, *Nucl. Instrum. Methods Sect. A* **286,** 1 (1990).
49. L. W. James, G. A. Antypas, J. Edgecumbe, R. L. Moon, and R. L. Bell, *J. Appl. Phys.* **42,** 4976 (1971).
50. S. F. Alvarado, F. Ciccacci, S. Valeri, M. Campagna, R. Feder, and H. Pleyer, *Z. Phys. B* **44,** 259 (1981).
51. B. Reihl, M. Erbudak, and D. M. Campbell, *Phys. Rev. B* **19,** 6358 (1979).
52. D. T. Pierce, G. C. Wang, and R. J. Celotta, *Appl. Phys. Lett.* **35,** 220 (1979).

53. C. J. Spindt, Ph.D. Thesis, Dept. of Applied Physics, Stanford University, Stanford, CA (1991).
54. I. Shiota, K. Motoya, T. Ohmi, N. Miyamoto, and J. Nishizawa, *J. Electrochem. Soc.* **124,** 155 (1977).
55. J. S. Escher, in *Semiconductors and Semimetals* (R. K. Willardson and A. C. Beer, eds.), Vol. 15. Academic Press, New York, 1981. p. 195.
56. Yu. G. Galitsyn, V. G. Mansurov, V. I. Poshevnev, and A. S. Terekhov, *Poverkhnost* Issue 10, 140 (1989).
57. Yu. G. Galitsyn, V. G. Mansurov, V. P. Opsheyenev, A. S. Terekhov, and L. G. Okorokova, *Poverkhnost* Issue 4, 147 (1989).
58. J. J. Uebbing, *J. Appl. Phys.* **41,** 802 (1976).
59. SAES Getters. Certain commercial instruments or materials are identified in this paper to clarify descriptions. In no case does such identification imply recommendation or endorsement by NIST.
60. W. Klein, *Rev. Sci. Instrum.* **42,** 1082 (1971).
61. C. Y. Su, W. E. Spicer, and I. Lindau, *J. Appl. Phys.* **54,** 1413 (1983); W. E. Spicer, Stanford University, Stanford, CA, private communication, September 1993.
62. D. C. Rodway and M. B. Allenson, *J. Phys. D* **19,** 1353 (1986).
63. B. J. Stocker, *Surf. Sci.* **47,** 501 (1975).
64. F. Ciccacci and G. Chiaia, *J. Vac. Sci. Technol., A* **9,** 2991 (1991).
65. G. H. Olsen, D. J. Szostak, T. J. Zamerowski, and M. Ettenberg, *J. Appl. Phys.* **48,** 1007 (1977).
66. V. Aebi, Intevac Corporation, private communication, September 1993.
67. C. C. Phillips, A. E. Hughes, and W. Sibbett, *J. Phys. D* **17,** 1713 (1984).
68. H. Tang, R. K. Alley, H. Aoyagi, J. E. Clendenin, J. C. Frisch, C. L. Garden, E. W. Hoyt, R. E. Kirby, L. A. Klaisner, A. V. Kulikov, C. Y. Prescott, P. J. Saez, D. C. Schultz, J. L. Turner, M. Woods, and M. S. Zolotorev, *Proc. Part. Accel. Conf.,* Washington, DC, *1993* Vol. 4, p. 3036 (1993).
69. A. Herrera-Gómez and W. E. Spicer, *Proc. SPIE—Int. Symp. Imaging Instrum.,* San Diego, *1993* (1993). p. 51.
70. M. Lax, *J. Appl. Phys.* **48,** 3919 (1977).
71. E. Mergl, E. Geisenhofer, and W. Nakel, *Rev. Sci. Instrum.* **62,** 2318 (1991).
72. F. C. Tang, M. S. Lubell, K. Rubin, A. Vasilakis, M. Eminyan, and J. Slevin, *Rev. Sci. Instrum.* **57,** 3004 (1986).
73. U. Kolac, M. Donath, K. Ertl, H. Liebl, and V. Dose, *Rev. Sci. Instrum.* **59,** 1933 (1988).
74. J. Frisch, R. Alley, M. Browne, and M. Woods, *Proc. Part. Accel. Conf.,* Washington, DC, *1993* Vol. 4, p. 3047 (1993).
75. U. Heinzmann, *J. Phys. E* **10,** 1001 (1977).
76. H.-J. Drouhin, C. Hermann, and G. Lampel, *Phys. Rev. B* **31,** 3872 (1985).
77. C. S. Feigerle, D. T. Pierce, A. Seiler, and R. J. Celotta, *Appl. Phys. Lett.* **44,** 866 (1984).
78. H.-J. Drouhin and P. Bréchet, *Appl. Phys. Lett.* **56,** 2152 (1990).
79. J. A. Simpson, *in* "Methods of Experimental Physics," Vol. 4A, (V. W. Hughes and H. L. Schultz, eds.) p. 124 Academic Press, New York, 1967.
80. J. D. Lawson, "The Physics of Charged-Particle Beams." Oxford Univ. Press (Clarendon), Oxford, 1977.
81. C. A. Sanford and N. C. MacDonald, *J. Vac. Sci. Technol., B* **8,** 1853 (1990);

C. A. Sanford, Ph.D. Thesis, Dept. Electrical Engineering, Cornell University, Ithaca, NY (1990).
82. D. J. Bradley, M. B. Allenson, and B. R. Holeman, *J. Phys. D* **10,** 111 (1977).
83. C. K. Sinclair and R. H. Miller, *IEEE Trans. Nucl. Sci.* **NS-28,** 2649 (1981).
84. C. A. Sanford and N. C. MacDonald, *J. Vac. Sci. Technol., B* **7,** 1903 (1989).
85. J. C. H. Spence, *Experimental High-Resolution Electron Microscopy*, p. 250. Oxford Univ. Press, Oxford, 1988.
86. V. Bargmann, L. Michel, and V. L. Telegdi, *Phys. Rev. Lett.* **2,** 435 (1959).
87. K.-H. Steffens, H. G. Andresen, J. Blume-Werry, F. Klein, K. Aulenbacher, and E. Reichert, *Nucl. Instrum. Methods A* **325,** 378 (1993).
88. D. A. Engwall, B. M. Dunham, L. S. Cardman, D. P. Heddle, and C. K. Sinclair, *Nucl. Instrum. Methods A* **324,** 409 (1993).
89. L. S. Cardman, *Nucl. Phys. A* **A546,** 317c (1992).
90. D. T. Pierce and R. J. Celotta, *in* "Optical Orientation" (F. Meier and B. P. Zakharchenya, eds.) p. 259, North-Holland Publ., Amsterdam, 1984.
91. T. Roder and E. Garwin, Stanford Linear Accelerator Center, Palo Alto, CA, private communication, 1979.
92. B. Schwartz, F. Ermanix, and M. H. Brastad, *J. Electrochem. Soc.* **123,** 1089 (1976).